Ultrasonics - Sonochemistry 42 (2018) 183–192

Contents lists available at ScienceDirect

Ultrasonics - Sonochemistry

journal homepage: www.elsevier.com/locate/ultson

A simple sonochemical approach to fabricate a urea biosensor based on zinc phthalocyanine/graphene oxide/urease bioelectrode

Sekar Selvarajan[a], Ayyadurai Suganthi[a,b,*], Muthuramalingam Rajarajan[c,*]

[a] PG & Research Department of Chemistry, Thiagarajar College, Madurai 625 009, Tamil Nadu, India
[b] Mother Teresa Women's University, Kodaikanal 624 102, Tamil Nadu, India
[c] Directorate of Distance Education, Madurai Kamaraj University, Madurai 625 021, Tamil Nadu, India

ARTICLE INFO

Keywords:
Nanocomposite
Urea
Bioelectrode
Cyclic voltammetry
Real samples

ABSTRACT

A novel zinc phthalocyanine/graphene oxide (ZnPh/GO) nanocomposite modified glassy carbon electrode (GCE) was prepared by using sonochemical approach and simple drop casting method. Urease (Urs) was used as the specific enzyme for urea detection and was physically immobilized onto the surface of ZnPh/GO nanocomposite. The fabricated ZnPh/GO/Urs matrix was successfully characterized by UV–vis-spectroscopy, FT-IR spectroscopy, scanning electron microscopy (SEM), raman spectrum, thermogravimetric analysis, cyclic voltammetric (CV) and amperometric techniques. The electrocatalytic performance of the ZnPh/GO/Urs electrode was investigated by urea biosensor. Our results demonstrate that the modified electrode has excellent electrocatalytic activity towards the sensing of urea in 0.1 M phosphate buffer solution (PBS, pH 7.2). The biosensor tolerated a wide linear concentration range for urea from 0.4 to 22 μM (R^2 = 0.991), with a detection limit of 0.034 μM (S/N = 3). The ZnPh/GO/Urs bioelectrode has several excellent properties, including a fast response time, high reproducibility and stability.

1. Introduction

Fertilizer plants and animal as well as human urine are supposed to be responsible for empowering urea in aqueous environment [1]. Higher urea level poses several adverse effect in the body including, renal failure, obstruction of urinary tract, bleeding issue in stomach and intestine, dehydration and shock burns while the lower urea level is responsible for nephritic syndrome, cachexia and hepatic failure [2]. In view of biological and environmental importance it is highly demanding to investigate urea concentration in clinical and environmental samples. Several diagnostic methods have been reported regarding urea determination in various types of samples including potentiometry [3,4], piezoelectricity [5], surface plasmon resonance [6] and molecularly imprinted polymer [7]. All these mentioned methods for urea determinations are faced with certain problems like use of several chemicals, less sensitivity, limited selectivity and expensive nature of material utilized for sensing application.

Phthalocyanies are aromatic macrocycles with a high electronic delocalization and an intense absorption in the red to near-IR zone [8]. They possess a great thermal, photochemical stability, electrocatalytic properties and are very versatile, since it is possible to change the central atom and to introduce substituents in the peripheral and axial positions, thus bringing the possibility to tune their physicochemical and optical properties [9]. In addition to their applications as photosensitizers for photodynamic therapy [10], as liquid crystals, [11] sensor [12] and in nonlinear optics [13] phthalocyanines have emerged with force in the field of photovoltaic devices.

Over the past few years, graphene (a one-atom-thick planar sheet of sp^2-bonded carbon atoms that are densely packed in a honeycomb crystal lattice) has attracted considerable research interest owing to its unique physical and chemical properties [14–16]. These properties suggest a wide-range of applications for graphene based materials such as adsorbents [17], catalyst supports [18], thermal transport media [19], electrode materials for electrochemical energy-storage devices (batteries/supercapacitors) [20] and components of biosensors [21]. Furthermore, ultrasound is accomplished due to the distinctive mechanisms and reaction pathways leading to a significant tool for chemistry became serious conditions. Recently, sonochemistry has been applied in the synthesis of functional nanoparticles and nanostructured materials. In this technique, the amount of energy is provided to the system via irradiation of a liquid with elevated intensity ultrasonic waves to facilitate produce regions of extreme temperature and pressure. Indeed, the sonochemical approach has allowed generating carbon supported nanoparticles with great uniformity whereas

* Corresponding authors at: Mother Teresa Women's University, Kodaikanal 624 102, Tamil Nadu, India (A. Suganthi).
E-mail addresses: suganthiphd09@gmail.com (A. Suganthi), rajarajan_1962@yahoo.com (M. Rajarajan).

https://doi.org/10.1016/j.ultsonch.2017.11.030
Received 4 October 2017; Received in revised form 20 November 2017; Accepted 21 November 2017
Available online 22 November 2017
1350-4177/

conventional preparation techniques do not provide sufficient control [22].

On the other hand, metallophthalocyanine (MPh) and metalloporphyrins belong to the classes of organometallic macrocycles, in particular zinc phthalocyanine has been well studied and showed an excellent electrocatalytic materials towards several important molecules such as red graps, carbamate, organophosphate, and various sensor [23–25]. Moreover, CoPh has also been used as redox mediators for enzyme based glucose sensors [26]. The ZnPh is not stable on the electrode surface due to its low conductivity along with poor electrochemical activity [27]. Hence the carbon nanomaterials [28], such as carbon nanotubes (CNTs) and graphene have been used with MPh to enhance the electrochemical conductivity and electron transfer of MPh and thus used for many potential applications including electrochemical sensors and biosensors [29–32]. Earlier studies revealed that GO is an ideal carbon nanomaterial to combine with MPh; more stable on the electrode surface due to the strong π–π interaction between MPh and GO [32]. The main aim of the present work is utilization of the special properties of the ZnPh/GO/Urs and used as an electrocatalyst for the sensing of urea.

Herein, we propose the sonochemical synthesis of ZnPh/GO nanocomposite modified GCE fabricated by the simple sonochemical and drop casting technique. This modified glassy carbon electrode have been further used to immobilize urease for urea detection via cyclic voltammetry technique. The fabricated bioelectrode showed good stability, specificity as well as reproducibility. The proposed ZnPh/GO/Urs biosensor showed a high sensitivity and a good detection limit compared to many other reports.

2. Experimental

2.1. Materials

Graphite powder (1–2 μm, synthetic) was obtained from Aldrich. Urease (urease enzyme, E.C.3.5.1.5 from Jack Bean 100 U mg^{-1}), Urea (ACS reagent 99.9%), zinc phthalocyanine and all chemicals used in this project were of analytical grade and purchased from Sigma Aldrich. The phosphate buffer solution (PBS) 0.1 M with a pH of 7.2 was prepared from Na_2HPO_4 and NaH_2PO_4. A stock solution of urea was prepared in 0.1 M PBS (pH of 7.2), and stored at 4 °C ultra-pure water was obtained from a Milli-Q water system.

2.2. Synthesis of graphene oxide

Graphene oxide was prepared using graphite according to the modified hummer's method [33] whereby 1 g of graphite powder was suspended in 2.5 g of $K_2S_2O_8$ and 46 ml of H_2SO_4 and then stirred in a round bottom flask at 0 °C for 15 min. Next, 2.5 g of P_2O_5 was added into the mixture and stirred vigorously for 6 h at 20 °C. On completion, the mixture was then poured and diluted with 1 L of water and filtered. Afterward, a 6 g of portion of $KMnO_4$ and 1 g of $NaNO_3$ in 31.2 ml of distilled water were added gradually while being stirred. The temperature of the mixture was controlled to below 20 °C. The reaction occurred as the mixture was stirred at 35 °C for 2 h, after which 500 ml of distilled water was added slowly to keep the temperature below 50 °C. After that further reaction was allowed to proceed for 2 h, and then 250 ml of water and 6 ml of H_2O_2 (30% weight) were added. The color of the mixture changed to brilliant yellow. Finally, the solid suspension was washed with a 2 M HCl solution and then washed 3–4 times with ethanol and dried in a vacuum at 60 °C overnight. The graphite oxide slurry was then dried in vacuum at 60 °C for 48 h before use.

2.3. Fabrication of urease immobilize ZnPh/GO modified GCE

ZnPh/GO nanocomposite modified electrodes was prepared by using a mixture of a slurry of ZnPh (4.3 mg) in ultra-pure Milli-Q water (1.5 mL) and 3.3 mg/mL suspension of GO that was ultrasonicated (irradiation power 75 W) for 30 min. 2μL of this mixture was dropped on the GCE electrode and kept to dry for 30 min at 80 °C. The freshly Urs solutions was prepared in PBS (phosphate buffer solution) and stored at 4 °C when not in use. Schematic illustration 1 provides an overview of the fabrication process of the urea sensor. Prior to use, covalently immobilize Urs on the as-prepared ZnPh/GO composite modified GCE, about 3 μl Urs was drop casted and allowed to dry at room temperature. For the one-step reaction, enzyme specific activity of 620 min^{-1} on membrane supports was seen to be comparable to solution enzyme specific activity of 10 min^{-1}. Thus, immobilization of Urs on the ZnPh/GO is highly favored through the electrostatic interactions. The obtained GC bioelectrode was then few times gently rinsed with doubly distilled water to remove the loosely bound Urs. The fabricated ZnPh/GO/Urs bioelectrode was used for further electrochemical experiments. All the electrochemical experiments were carried out at room temperature. Preparation of GC/GO electrodes without ZnPh was obtained according to the same procedure, using only functionalized GO (without mixing with ZnPh). The overall experimental synthesis mechanisms are clearly documented in Scheme 1.

2.4. Apparatus

Electrochemical experiments were carried out using a CH-660E Instruments electrochemical work station (CH Instruments, Texas, USA). The Three – electrode system consisted of a bare GCE 0.079 cm^{-2} geometrical surface area) or ZnPh/GO/Urs bioelectrode as working electrode, an Ag/AgCl as a reference electrode (saturated KCl) and platinum wire as a counter electrode. The potentials mentioned in all experimental results were referred to standard Ag/AgCl (saturated KCl) reference electrode. SEM measurements were carried out at VEGA3 TESCAN, USA. Raman spectra were measured with a Raman spectrometer (Dong woo 500i, Korea) equipped with a charge-coupled detector. TGA of samples was carried out with a TGA-50, SHIMADZU thermogravimetric analyzer at a heating rate of 10 °C min 1 up to 800 °C under nitrogen. Fourier transform infrared (FT-IR) measurements were performed using a Perkin Elmer spectrophotometer RXI. Hitachi U-3300 spectrophotometer was used to carry out UV–visible absorption spectroscopy measurements. The crystalline structure of the nanoparticles was studied by an X-ray diffraction (XRD; XPERT PRO X-RAY) with Cu Kα radiation at 25 °C and the structural assignments were made with reference to the JCPDS power diffraction files (Scheme 2).

3. Results and discussion

3.1. UV–vis-spectroscopy

The UV–vis absorption spectra of GO, ZnPh, ZnPh/GO, and urease immobilize/ZnPh/GO are displayed in Fig. 1. Absorption spectra of GO (Fig. 7a) indicated the characteristics absorption band near to 230 nm due to $\pi \rightarrow \pi*$ transition of aromatic ring electrons and a small hump near to 300 nm due to $n \rightarrow \pi^*$ of carbonyl groups [33]. As shown in Fig. 7b, ZnPh exhibit three main characteristic absorption peaks, such as B band at 320 nm in ultraviolet band, Q bands at 612 nm and 676 nm in visible region, respectively. This is confirms the formation of ZnPh [34]. After the addition of ZnPh onto the surface of GO, the absorbance was shifted from 328 to 678 nm, which is due to Q band absorption of ZnPh was (Fig. 7c) confirmed by on the surface of GO. Finally, Urs was further added to on the surface of ZnPh/GO hybrid shows three characteristic absorption bands are observed, such as 322 nm, 621 nm and 682 nm respectively. It was confirmed by successfully fabricate Urs on the surface of ZnPh/GO nanocomposite (Fig. 7d).

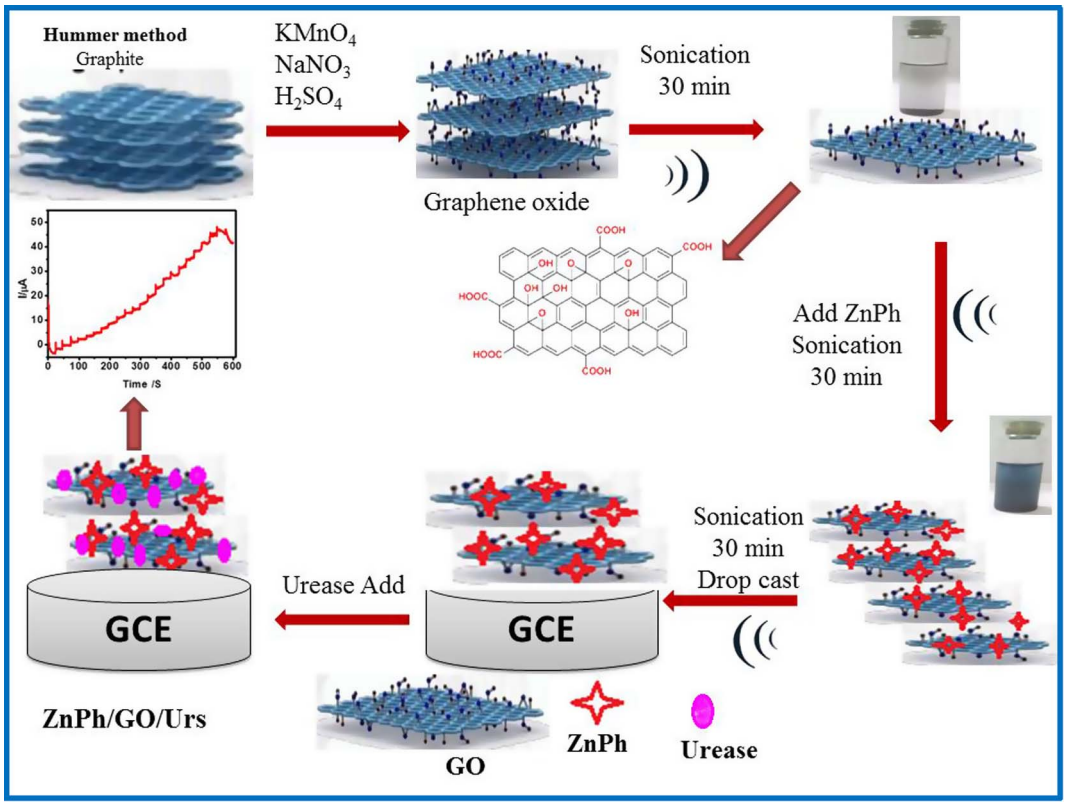

Scheme 1. Schematic illustration of the preparation of ZnPh/GO/Urs modified GC bioelectrode.

3.2. FT-IR

The FT-IR spectra of (a) GO, (b) ZnPh/GO and (c) urease immobilize ZnPh/GO are shown in Fig. 2. The GO exhibited bands at 3408, 1721, 1620, 1220 and 580 cm^{-1} due to the stretching mode of O—H, C═O, C═C, C—O and C—O—C bands, respectively which can be clearly observed in the FT-IR spectrum [34]. After the addition of ZnPh on the surface of GO, the characteristic absorption of C═O stretching vibration appears at 1646 $cm^{-1}$of ZnPh can clearly observed in the spectrum of ZnPh/GO nanocomposite [35]. The FT-IR spectrum after immobilization of urease over ZnPh/GO nanocomposite shows some additional bands at 1645 cm^{-1} (corresponding to N—H stretching in amide II) and 999 cm^{-1} (assigned to C—O stretching) due to presence of amide bond revealing immobilization of Urs onto nanocomposite. The results confirmed the effective loading of immobilized urease on the surface of ZnPh/GO composite matrices by the physical adsorption technique [36].

3.3. X-ray diffraction

The XRD profiles of GO, ZnPh/GO and urease immobilize ZnPh/GO composite are shown in Fig. 3. The characteristic diffraction peak of GO (Fig. 3a) is appeared at 10.8° corresponding to the 0 0 1 plane. After immobilization of ZnPh on the surface of GO, when the peak disappeared and another broad diffraction newly peak 26° (0 0 2) appeared is shown in Fig. 3b [35]. Further added Urs on the surface of ZnPh/GO composite at peak intensity was decreased as shown in Fig. 3c. This is due to the significant interaction between ZnPh, GO and Urs respectively. The average crystalline sizes of pure ZnPh/GO composite and urease immobilize ZnPh/GO nanocomposite calculated by Debye – Scherrer formula were found to be 12 to 20 nm [37].

3.4. Raman spectroscopy

Raman spectroscopy is a powerful method for studies on conjugated

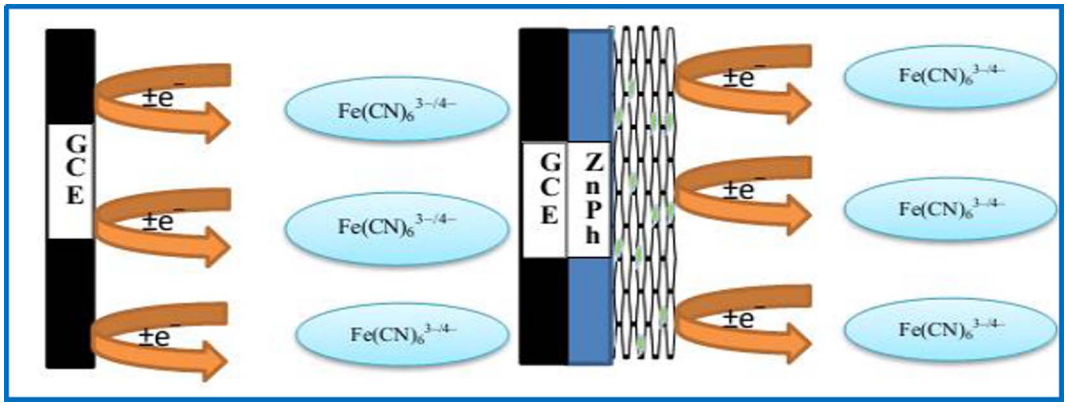

Scheme 2. Schematic of the mechanistic model proposed for electron transfer at ZnPh/GO/Urs biosensor in free urea PBS (pH 7.0) containing 5 mM $[Fe(CN)_6]^{3-/4-}$.

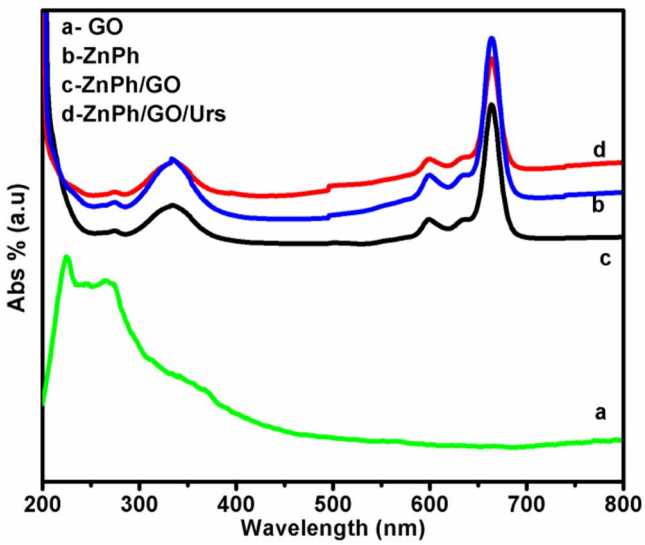

Fig. 1. UV–vis-spectrum of a) GO, b) ZnPh c) ZnPh/GO, and ZnPh/GO/Urs.

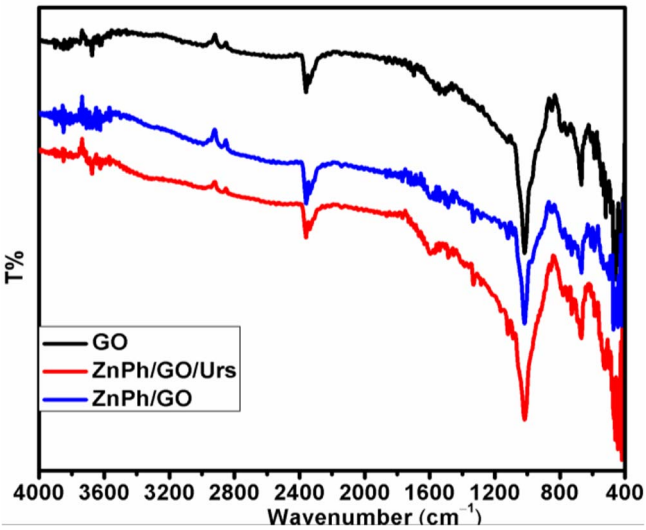

Fig. 2. FTIR spectrum of a) GO, b) ZnPh c) ZnPh/GO, and ZnPh/GO/Urs.

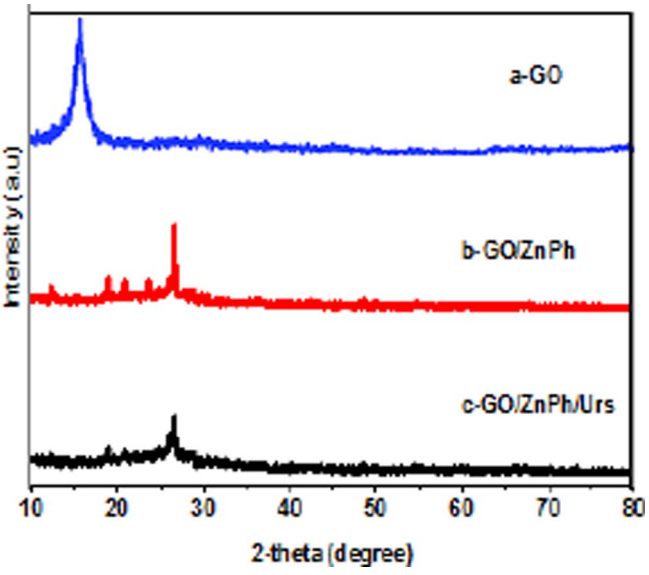

Fig. 3. XRD pattern of a) GO, b) ZnPh/GO, and ZnPh/GO/Urs.

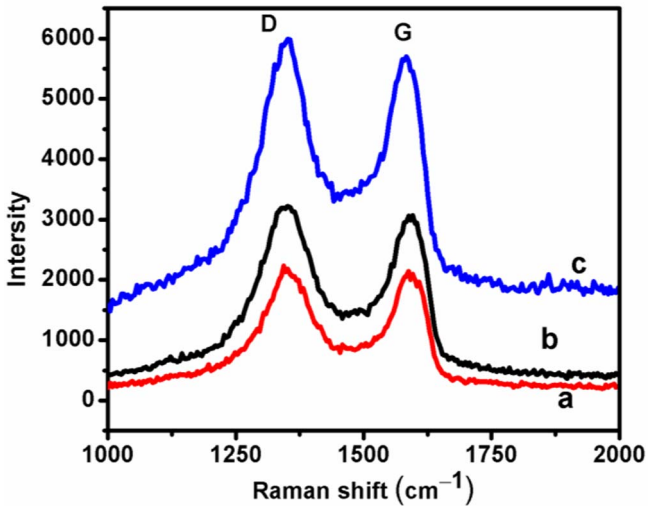

Fig. 4. Raman spectra of a) GO, b) ZnPh/GO, and ZnPh/GO/Urs.

carbon sp^2-hybridized bonds as shown in Fig. 4. As cab be seen that GO, ZnPh/GO nanocomposite and urease immobilize ZnPh/GO composite of raman signals intense G band and D band located at 1354 cm^{-1}, 1583 cm^{-1} [36]. The Raman spectral band intensity ratio [I_D/I_G] of GO, ZnPh/GO and urease immobilize ZnPh/GO composite are observed at 0.89, 1.10 and 1.30, respectively. Herein urease immobilized ZnPh/GO band intensity ratio was increased when compared to GO, and ZnPh/GO. This is an agreement with that of XRD results above.

3.5. Thermogravimetric analysis

Supporting evidence for the structure of nanomaterial was suggested by thermal analysis of GO, ZnPh/GO and urease immobilize ZnPh/GO composite are shown in Fig. 5. The TGA measurement of all the nanomaterials was performed in air oven at a temperature range of 25–800 °C. On the other hand, the TGA graph of GO, ZnPh/GO and urease immobilize ZnPh/GO revealed a 41%, 19% and 24% weight loss, in the temperature range of 200–500 °C, which is attributed to the thermal decomposition of ZnPh functionally attached to graphene oxide. The weight loss that occurred above 500 °C is attributed to the thermal decomposition of defects created at sites where graphene

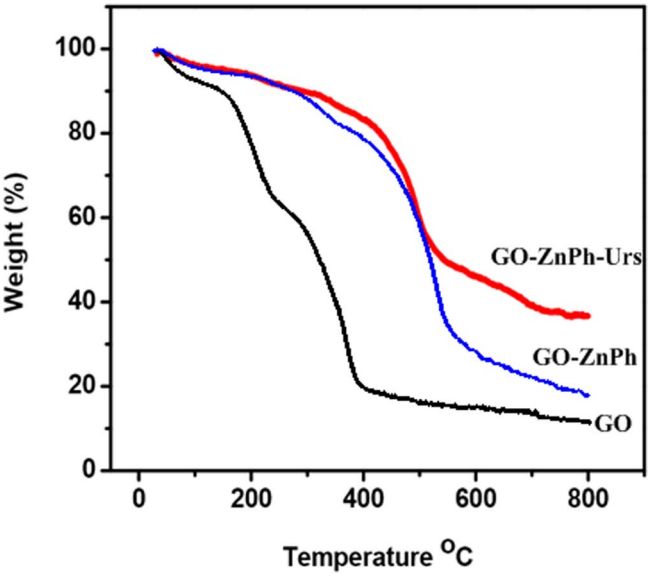

Fig. 5. TGA of GO, ZnPh/GO and ZnPh/GO/Urs.

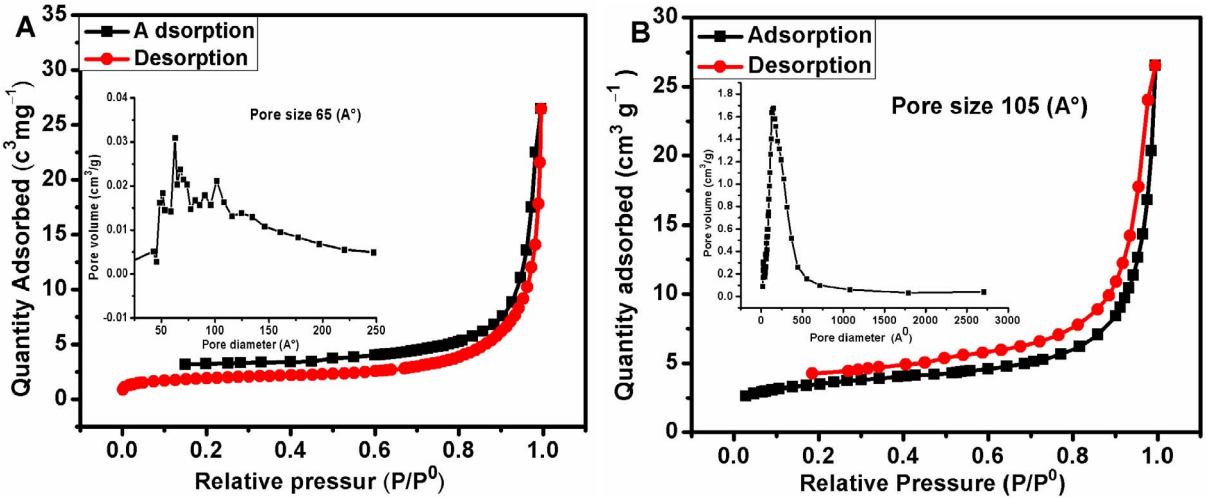

Fig. 6. N_2 adsorption-desorption isotherm and Barrett–Joyner–Halenda (BJH) pore size distribution plot (inset) of Urease modified GO/ZnPh nanocomposite.

functionalization took place [36].

3.6. BET

The pore structure of ZnPh/GO and urease immobilize ZnPh/GO composite have been investigated by N_2 adsorption-desorption isotherm at −196 °C. The corresponding pore size distribution and specific surface area were determined using the BJH method and BET method respectively. The N_2adsorption-desorption isotherm and pore size distribution curve were shown in Fig. 6. The isotherms (Fig. 6A and B) are identified as of Type IV. It is characteristic of mesoporous materials according to the IUPAC classification [37]. A sharp increase in adsorption volume of N_2 was observed and located in the P/P° is 0.99. This sharp increase can be attributed to the capillary condensation, indicating the good homogeneity of the sample and macro size because the P/P_0 position of the inflection point is related to the pore size. Average pore radius of ZnPh/GO composite and urease immobilize ZnPh/GO composite are shown by pore size distribution curve in the inset of Fig. 6, are 65 Å and 108 Å. The pore size distribution on the sample thus conform the mesoporous structure [38]. Surface area measurements, made by the BET method, provide the specific surface area of ZnPh/GO composite and urease immobilize ZnPh/GO biocomposite are 24.96 $m^2 g^{-1}$ and 35.65 $m^2 g^{-1}$. The single point adsorption total pore volume of pore < 2525.70 Å radius at $P/P_0 = 0.991$ is 0.91 cm^2/g. Moreover, it has to be emphasized that this type of isotherm indicates the presence of mesoporous structure in urease immobilize ZnPh/GO biocomposite.

3.7. Scanning electron microscopy (SEM)

SEM image of GO, ZnPh/GO and urease immobilize ZnPh/GO biocomposite are displayed in Fig. 7. The surface morphology of bare GO has a typically folded and sheet like structure, which looks like soft and thin gauze. An SEM micrograph of the hybrid nanocomposite matrix of ZnPh/GO looks very similar to that of GO. After immobilization of Urs on the surface of ZnPh/GO film observed the sheet like structure changes to regular form.

3.8. Electrochemical behavior of urease immobilized ZnPh/GO modified electrode

A schematic of the proposed mechanism for electron transfer at the urease immobilize ZnPh/GO bioelectrode in urea free PBS (pH 7.2) containing 5 mM $[Fe(CN)_6]^{3-/4-}$ redox probe is shown in schematic 2. Fig. 8A shows CV obtained for (a) bare (b) ZnPh (c) ZnPh/GO and urease immobilized ZnPh/GO bioelectrode in urea free PBS (pH 7.2) containing 5 mM $[Fe(CN)_6]^{3-/4-}$ redox probe at a scan rate of 0.1 Vs^{-1}. The anodic potential (a–d) shifts towards a higher current and the cathodic peak potential shifts in the opposite direction. In reference to the ZnPh/GC electrode surface, oxidation and reduction peaks are obtained at 0.41 and −0.31 V, respectively (curve b), which is found to be increased when compared to that of the bare GCE (curve a). This increase is a result of the cationic characteristics of ZnPh, which accepts electrons from the medium and transfer them to the electrode [39]. The magnitude of the response current is increased for the ZnPh/GO/Urs bioelectrode (curve d) is compared to other modified electrode (curve a–c); which is due to redox properties of the synergistic effect of Urs with ZnPh/GO [40].

Cyclic voltammograms at the scan of 0.1 Vs^{-1} obtained for (a) bare GCE (b) ZnPh/GCE (c) ZnPh/GO/GCE (d) ZnPh/GO/Urs/GCE in PBS (pH 7.2) containing 10 mg L^{-1} urea in the absence of 5 mM $[Fe(CN)_6]^{3-/4-}$ are shown in Fig. 8B. By comparing curve 'a and b', it can be observed that an anodic peak is appeared to ZnPh modified GCE in the presence of urea, which is due the partial hydrolysis of urea at the ZnPh/GCE. The magnitude of anodic peak current responses is increase greatly by ZnPh/GO/Urs bioelectrode (curve d) compared to others [41,42].

The electrochemical impedance spectroscopy (EIS) date obtained for a) bare b) ZnPh/GO/Urs modified GC bioelectrode in free urea containing 0.1 M PBS presence of 5 mM $[Fe(CN)_6]^{3-/4-}$ (pH 7.2) as shown in Fig. 9. The charge transport process of the ZnPh/GO/Urs modified GC bioelectrode was studied by monitoring charge transfer resistance (Rct) at the electrode/electrolyte interface. The R_{ct} value was obtained by randles equivalent circuit $[R_S(Q_{CPE}\ (R_{ct}\ W)]$, where R_S is the solution resistance, W is the warburg impedance and Q_{CPE} is the constant phase element (CPE). The R_{ct} values for bare GCE (curve a) and ZnPh/GO/Urs (curve b) bioelectrode have been estimated as 1386 and 21,689 Ω/cm^2 respectively.

The effect of the scan rate on the redox currents of Urea for the ZnPh/GO/Urs bioelectrode is shown Fig. 10 (10 mM L^{-1} urea in the absence of 5 mM $[Fe(CN)_6]^{3-/4-}$). It can be observed that the redox peak currents both increased at higher scan rates, and the response current was linearly proportional to the scan rate in the range of 10 to 100 mV^{-1}. The linear regression equation for the cathodic peak current was I_{pc} (μA) = 1.947x + 18.423 (mVs^{-1}), with a correlation coefficient of $R^2 = 0.9912$, and for the anodic peak current it was I_{pa} (μA) = −1.967x − 12.423 (mVs^{-1}), with a correlation coefficient of $R^2 = 0.9922$. This indicates that the contribution of adsorption played a key role in the electrode reaction, owing to the fact that the affinity and the surface accumulation process of urea was slow on the ZnPh/GO/Urs

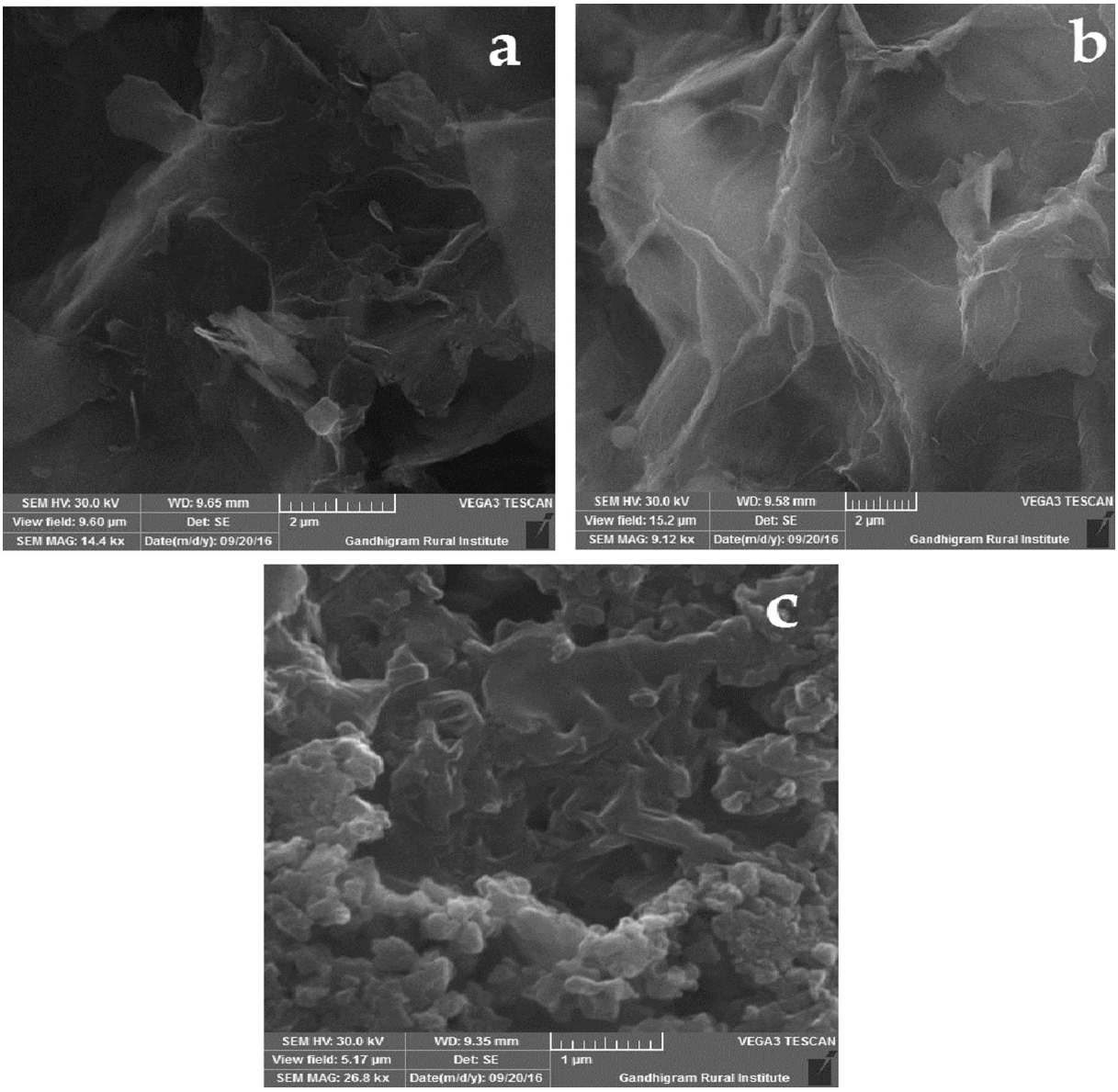

Fig. 7. SEM image of a) GO b) ZnPh/GO and ZnPh/GO/Urs.

bioelectrode. The suggest that the overall oxidation and reduction of urea at ZnPh/GO/Urs bioelectrode is controlled by an adsorption phenomenon.

Fig. 11 shows the CV response of the ZnPh/GO/Urs bioelectrode upon the successive addition of urea in the PBS (pH 7.2) solution. It can be seen that the oxidation Hence, the catalytic oxidation of urea by the immobilized urease involves gain or loss of electrons thus completing a redox reaction and the observed increase in the oxidation peak current with increasing concentration of urea is attributed to the increase in the number of released electrons during oxidation current of the bioelectrode increases linearly range from 71 µA to 125 µA with increasing urea concentration from 1 mg to 12 mg dL^{-1} (inset Fig. 11) with a correlation coefficient (R) of 0.99, indicating good electrocatalytic behavior of the ZnPh matrix.

Fig. 12 shows the amperometric response of the ZnPh/GO/Urs bioelectrode to successive step-wise additions of urea to 0.1 M PBS. A significant increase in peak current was observed when urea was added to the stirred 0.1 M PBS solution. The electrode exhibited a rapid response to the urea, reaching a plateau within 10 s. Fig. 12 inset shows the calibration curve for the measurement of the urea. The electrode showed a linear relationship with the concentration (0.4–22 µM) using a regression equation of I(mA) = 0.370x + 0.2338 C. The detection limits (DL) for the bioelectrode have been calculated using the following expression [42].

$$DL = (3 \times SD)/S$$

where SD is the standard deviation in peak oxidation current and S is the sensitivity of the electrode towards urea. The detection limit of urea is found to be 0.034 µM, response time is 10 s and sensitivity is 44.53 µA mM^{-1}. Finally, based on the enzyme electrostatic immobilization strategy, the response characteristics of the ZnPh/GO/Urs bioelectrode with the other reported urea biosensors was compared and summarized in Table 1.

The value of the Michaelis–Menten constant (km) has been obtained as 3.2 mg/dL using Lineweaver–Burke plot. The observed low K_m value reveals the higher affinity of ZnPh/GO/Urs bioelectrode and is attributed to favorable orientation of Urs and higher loading of Urs provided by the microenvironment of ZnPh/GO nanocomposite [43].

3.9. Sensing mechanism

The mechanism of urea sensing can be explained based on the two

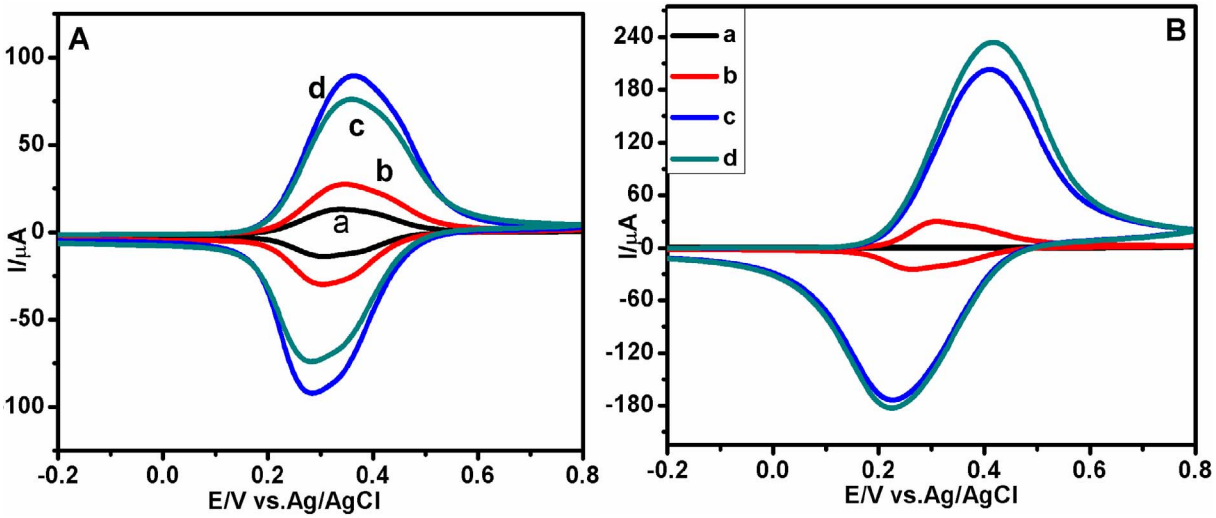

Fig. 8. A Cyclic voltammograms at the scan of 0.1 Vs^{-1} obtained for a) bare GCE b) ZnPh/GCE c) ZnPh/GO/GCE d) ZnPh/GO/Urs/GCE in urea free PBS (pH 7.2) containing 5 mM $[Fe(CN)_6]^{3-/4-}$ redox probe. B Cyclic voltammograms at the scan of 0.1 Vs^{-1} obtained for a) bare GCE b) ZnPh/GCE c)ZnPh/GO/GCE d) ZnPh/GO/Urs/GCE in PBS (pH 7.2) containing 10 mg L^{-1} urea in the absence of $[Fe(CN)_6]^{3-/4-}$ probe.

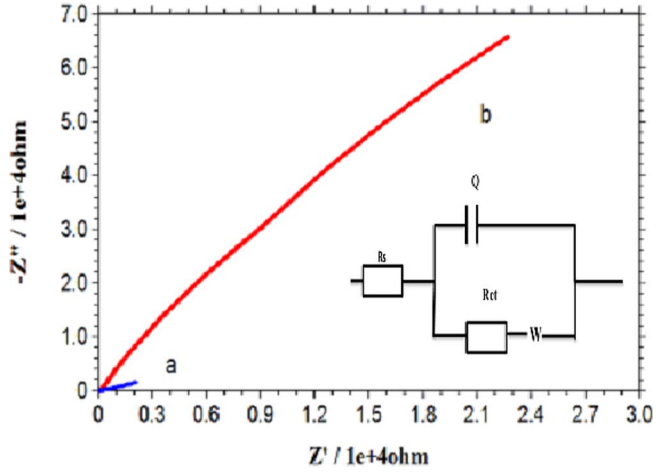

Fig. 9. The Nyquist plot (− Z′ vs Z′) of a) bare GCE b) ZnPh/GO/Urs/GCE in urea free PBS (pH 7.2) presence of 5 mM $[Fe(CN)]^{3-/4-}$.

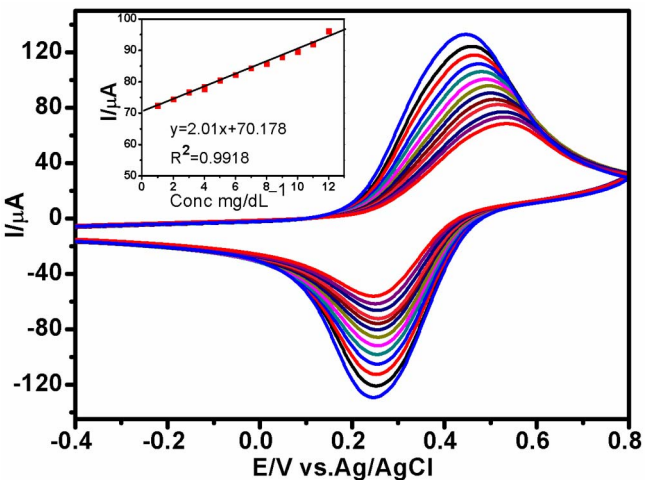

Fig. 11. Electrochemical CV response studies of ZnPh/GO/Urs modified GC bioelectrode as a function of urea concentration (1 mg to 12 mg dL^{-1}).

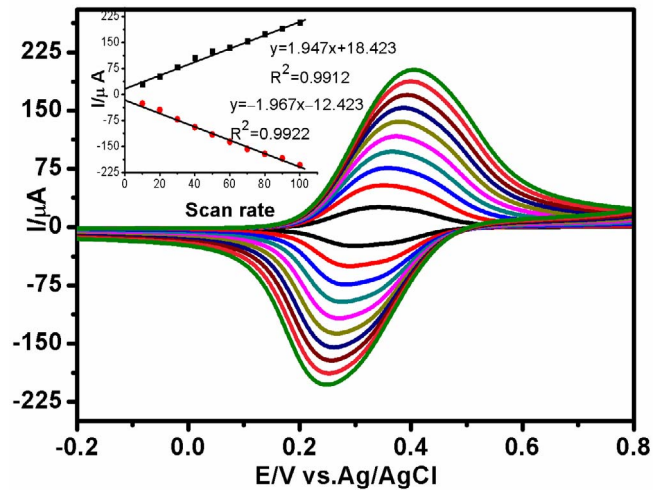

Fig. 10. CV of the ZnPh/GO/Urs modified GC electrode at different scan rates in 10 mM L^{-1} urea in the absence of 5 mM $[Fe(CN)_6]^{3-/4-}$ probe (10–100 mVs^1) (Inset redox peaks current as function of square root of scan rate).

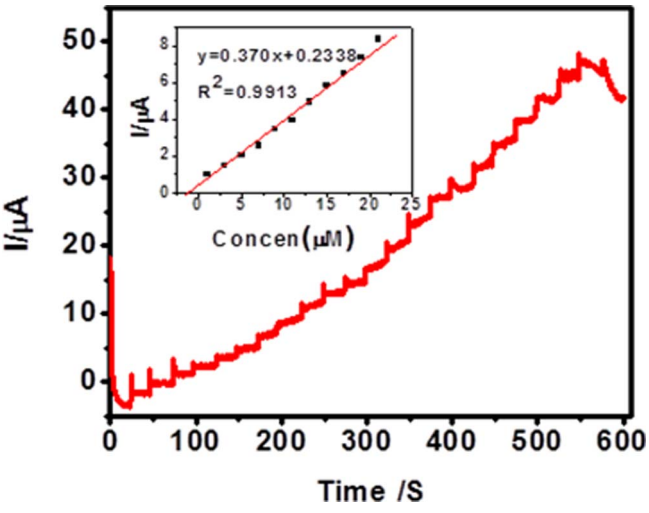

Fig. 12. Schematic representation of the detection mechanism of ZnPh/GO/Urs modified GC bio electrode for urea sensor.

Table 1
A comparative table describing the urea sensing characteristics of the ZnPh/GO/Urs modified GC bioelectrode along with some other reported in the literature.

Electrode	Linear Range	Detection limits	Stability	Detection method	Response time (s)	Ref.
Graphene based FET	1–1000 μm	1 μM	–	Amperometric	1	[49]
ITO/SG-PANI/Urs	0.12–12.3 mM	0.050 mM	15 days	Amperometric	5	[50]
Full-U/SPE 3	1.2–0.042 mM	5×10^{-4} M	5 months	Potentiometric	1	[51]
UCPHM GCE	1.55–1000 μM	60 nM	4 weeks	DPV	10	[52]
Graphite and platinum composite electrode	10–250 μ M	3 μM	3 months	Amperometric	3	[53]
Urs-GLDH/MLG/ITO	10–100	3.9 μM	2 months	Cyclic Voltammetry	10	[54]
FTO/ZnO polymer/Urs	5–125 mg	3 mg	4 month	Amperometric	3	[45]
FTO/ZnO/Urs	8–110 mg	5 mg	3 weeks	Amperometric	10	[55]
$NiCo_2O_4$/3D graphene/ITO	0.06–0.30 mM	5.0 μM	4 months	Amperometric	1	[56]
Urs-GLDH/GOS/ITO	3.3–19.9 mM	2.1 mM	5 weeks	Cyclic Voltammetry	–	[57]
ZnPh/GO/Urs/GC	0.4–22 μM	0.034 μM	8 weeks	Amperometric	10	This work

reactions viz. (i) catalytic reaction and (ii) oxidation/reduction of carbon based nanomaterilas; same as that of solid state gas sensors. The catalytic reaction of urea–urease is well known which produces three ions i.e. two NH_4^+ and CO_3^- from uncharged urea [44]. These produced ions increase the conductivity of the host material by providing excess electron to the conduction band of the material.

The second process for the oxidation/reduction of metal oxides, which occurs due to the adsorbed oxygen and the catalytically produced excess ions, can be explained as below. Many researchers clarify the modification in the electrical conductance of a highly porous semiconducting material sensor in the presence of toxic gases due to the reactions occurring on the surface. Fig. 13 shows the mechanism at first, atmospheric oxygen molecules are physisorbed on the surface sites, which get ionized by extracting an electron from the conduction band while moving from one site to another, and are thus ionosorbed on the surface as O_{ads}^-. This leads to a decrease in the conductance of the transducer, as indicated by an increase in potential barrier at the grain boundaries as illustrated in Fig. 13a.

Upon exposing ZnPh/GO/Urs bioelectrode to urea, an enzymatic reaction takes places between Urs and urea which can be represented as Fig. 13b [44–47].

$$NH_2CONH_2 + 2H_2O \xrightarrow{Urs} NH_4^+ + CO_3^{2-} \quad (4)$$

$$R + O_{ads}^- \longrightarrow RO + e^- \quad (5)$$

As indicated in Eq. (4), NH_4^+ ion, which reacts with the surface adsorbed oxygen (O_{ads}^-) and thereby release the trapped electron to the conduction band of ZnPh/GO as indicated by the decrease of potential barrier at grain boundary as shown in Fig. 13c. Further, when reducing gas (R) molecules (ammonia in the present case) react with pre-adsorbed negatively charged oxygen adsorbates, the trapped electrons are given back to conduction band of the material. The energy released during the decomposition of adsorbed ammonia molecules would be sufficient for the electrons jumping up into the conduction band so as to increase conductivity of the biosensor.

The strength and performance of the enzyme on the matrix surface powerfully depends on the immobilization and surface chemistry. Among the several immobilization techniques, covalent attachment of the biomolecule to the substrate is one of the most stylish immobilization methods. The optimum buffer pH for hydrolysis of urea by Urs was considered as 7.2 at which Urs enzyme retains its maximum activity and natural structure that is required to improve detection limit and sensitivity for urea detection. Subsequently during this reaction the urease gets reduced. The activity of urease is due to the presence of SH groups on its active site that can be oxidized as well as reduced by the biochemical reactions. Hence, the reduced urease loses electrons and gets oxidized [40,48].

3.10. Reproducibility, stability and specificity

The ZnPh/GO/Urs modified GC bioelectrode for urea biosensor has been checked for its accountability by different tests such as reproducibility, specificity and stability measurements (Fig. 14). The reproducibility of ZnPh/GO/Urs bioelectrode has been determined by monitoring the maximum peak current response for the five similar electrodes made using the same protocol. It is found that there is no major change in the peak current response (see Fig. 14a) and conforms the reproducibility of the ZnPh/GO/Urs bioelectrode as a reliable urea biosensor. The stability of the biosensor was monitored for a period of eight weeks at an interval of one week to see the peak current response change with respect to aging. There was only ~6% decrease even after the eight week period when stored under refrigerated conditions (4°C) (Fig. 14b). Further the ZnPh/GO/Urs bioelectrode urea biosensor's specificity towards urea has been measured to see the response with other analytes. For this, the interference monitored by checking the peak current response of ZnPh/GO/Urs bioelectrode in comparison with other interferants such as urea, glucose, cholesterol, uric acid, ascorbic acid and lactic acid. The absence of similar peak current response as in the case of urea is an indication of the high specificity of the ZnPh/GO/Urs bioelectrode towards urea (Fig. 14c).

Several assays were made on blood serum to test the precision of the ZnPh/GO/Urs bioelectrode. The urea concentration was determined by the calibration curve (Table 2). Corresponding experiments were carried out with a spectrophotometric method by a local hospital. The results exhibited good consistent and precision between the two methods confirmed the proposed method is useful for application in real samples with good precision and accuracy.

Our results of using a drop casting ZnPh/GO/Urs bioelectrode based urea biosensor (this work) compared with the electrostatic adsorption based biosensors showed adequate efficiency of the semiconductor based biosensors with respect to the other types of used substrates. It can be postulated that the semiconductor substrate showed good linear range, low detection limit, and fast response time. The fast response time can be related to the faster electron transfer at the electrode surface as explained in the proposed mechanism.

4. Conclusion

In summary, ZnPh/GO nanocomposite modified GC electrode has been used to immobilize Urs fabricate electrochemical urea biosensor. ZnPh/GO/Urs bioelectrode displays excellent catalytic property to urea due to increased active site of nanocomposite by GO and provides friendly microenvironment for high loading of Urs resulting in enhanced electron transport between analyte and ZnPh/GO/Urs bioelectrode surface. ZnPh/GO/Urs bioelectrode exhibits sensing characteristics such as shows linearity of 0.4–22 mM, lower detection limit of 0.034 mM, response time of 10 s and sensitivity of 44.53 μA mM^{-1}. Efforts should be made to fabricate other biosensors based on this interesting nanocomposite. Moreover, the platform was highly regenerable and could be used 5 times without requiring any substantial alteration to the measurements. Measurements on such platforms were also found to be advantageous in many respects as they were very

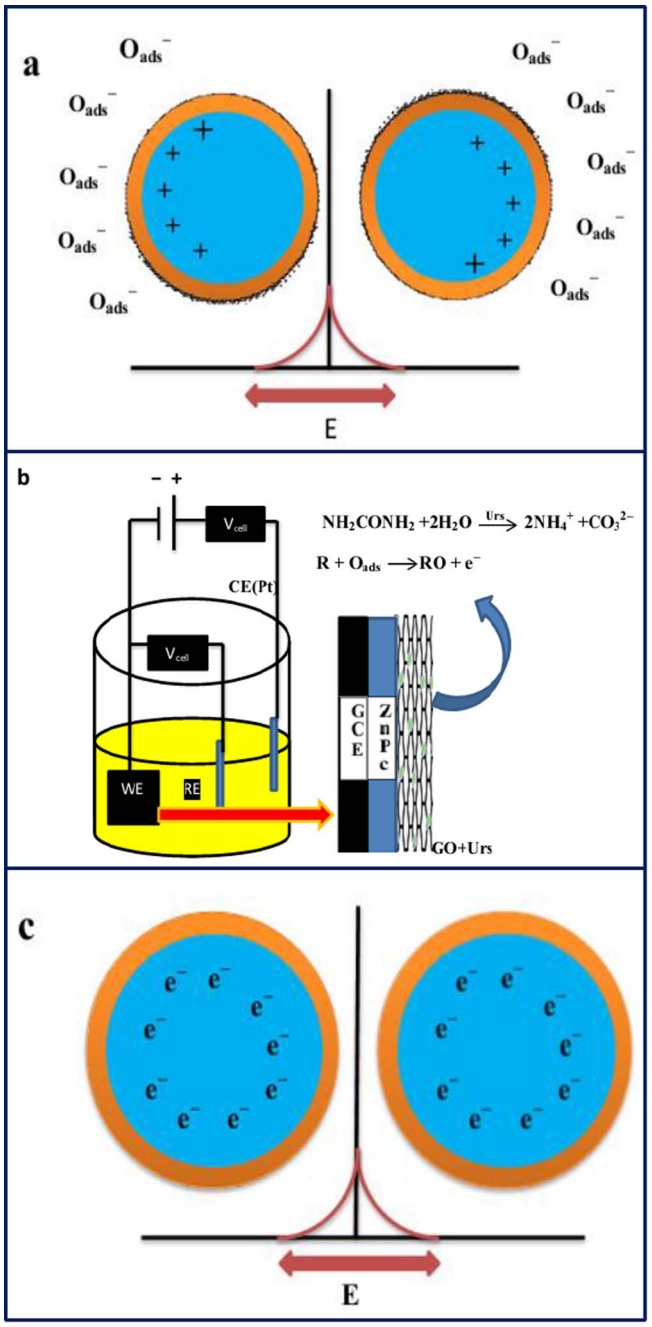

Fig. 13. a) Different ZnPh/GO/Urs modified GC bioelectrode fabricated via the conditions applied to conduct the reproducibility test. (b) Stability studies of the ZnPh/GO/Urs bioelectrode measured at a regular interval of one week up to eight weeks. (c) specificity plot describing the CV response of the ZnPh/GO/Urs modified GC bioelectrode in the presence of urea, cholesterol, glucose, uric acid, ascorbic acid and lactic acid.

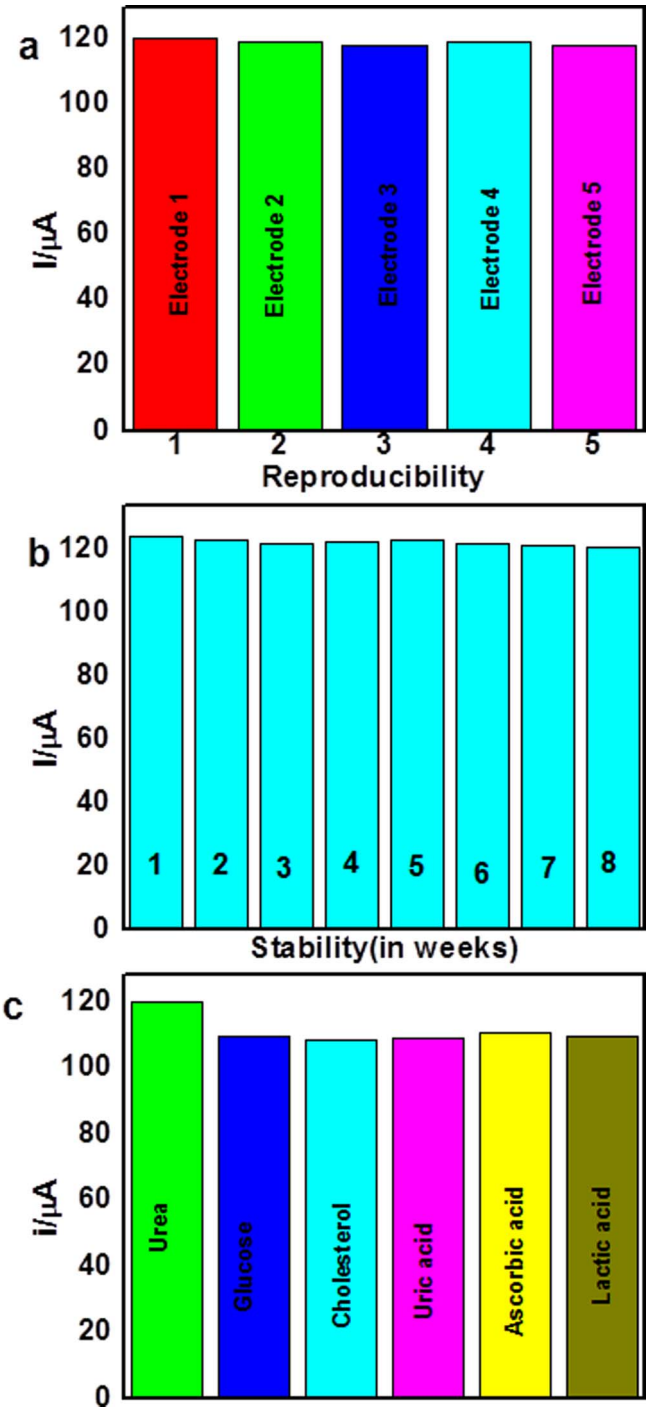

Fig. 14. a) ZnPh/GO/Urs bioelectrodes conduct the reproducibility b) Stability of the ZnPh/GO/Urs bioelectrode measured at a regular interval of one week upto 8 week c) Specificity plot describing the CV response of the ZnPh/GO/Urs bioelectrode in the presence of urea, glucose, cholesterol, uric acid, ascorbic acid, lactic acid.

simple, reproducible, and reliable. The development of such a platform was advancement with regard to the development of a new generation of sensors

Acknowledgements

The authors are grateful to DST-SERB (SB/S1/IC-06/2013 dt:03/09/2014) India for providing financial support. The Management of Thiagarajar College is acknowledged for providing necessary laboratory facilities.

Table 2
Determination of urea level in blood serum.

Method	Sample number				
	1	2	3	4	5
Determined by spectrophotometry (mM dL^{-1})	2.97	4.65	3.12	1.56	5.34
ZnPh/GO/Urs modified GC bioelectrode	2.95	4.60	3.11	1.53	5.31

References

[1] F. Guo, K. Ye, K. Cheng, G. Wang, D. Cao, Preparation of nickel nanowire arrays electrode for urea electro-oxidation in alkaline medium, J. Power Source 278 (2015) 562–568.
[2] A. Kaushika, P.R. Solanki, A.A. Ansari, G. Sumana, S. Ahmad, B.D. Malhotra, Iron oxide-chitosan nanobiocomposite for urea sensor, Sens. Actuat. B 138 (2009) 572–580.
[3] C.C. Buron, M. Quinart, T. Vrlinic, S. Yunus, K. Glinel, A.M. Jonas, B. Lakard, Application of original assemblies of polyelectrolytes, urease and electrodeposited polyaniline as sensitive films of potentiometric urea biosensors, Electrochim. Acta 148 (2014) 53–61.
[4] E.M. Basova, M.A. Bulanova, V.M. Ivanov, Photometric detection of urea in natural waters, Moscow Univ. Chem. Bull. 66 (2011) 345–350.
[5] Z.-P. Yang, X. Liu, C.-J. Zhang, B.-Z. Liu, A high-performance nonenzymatic piezoelectric sensor based on molecularly imprinted transparent TiO_2 film for detection of urea, Biosens. Bioelectron. 74 (2015) 85–90.
[6] P. Bhatia, B.D. Gupta, Fabrication and characterization of a surface plasmon resonance based fiber optic urea sensor for biomedical applications, Sens. Actuat. B 161 (2012) 434–438.
[7] T. Alizadeh, A. Akbari, A capacitive biosensor for ultra-trace level urea determination based on nano-sized urea-imprinted polymer receptors coated on graphite electrode surface original, Biosens. Bioelectron. 43 (2013) 321–327.
[8] S. Hu, R. Tian, Y. Dong, J. Yang, J. Liu, S. Cao, Preparation and optical properties of phthalocyanine–carbon dot blends, RSC Adv. 3 (2013) 21447–21452.
[9] M. Shi, Y. Zhao, H. Xu, J. Mack, L. Yin, X. Wang, Z. Shen, Photoisomerization and optical properties of a subphthalocyanine–azobenzene–subphthalocyanine triad, RSC Adv. 6 (2016) 71199–71205.
[10] A.M. Master, M. Livingston, N.L. Oleinick, A.S. Gupta, Optimization of a nanomedicine-based silicon phthalocyanine 4 photodynamic therapy (Pc 4-PDT) strategy for targeted treatment of EGFR-overexpressing cancers, Mol. Pharmaceut. 9 (2012) 2331–2338.
[11] H. Hayashi, W. Nihashi, T. Umeyama, Y. Matano, S. Seki, Y. Shimizu, H. Imahori, Segregated donor–acceptor columns in liquid crystals that exhibit highly efficient ambipolar charge transport, J. Am. Chem. Soc. 133 (2011) 10736–10739.
[12] A. Kumar, J. Brunet, C. Varenne, A. Ndiaye, A. Paulya, Phthalocyanines based QCM sensors for aromatic hydrocarbons monitoring: Role of metal atoms and substituents on response to toluene, Sens. Actuat. B 230 (2016) 320–329.
[13] C.-B. Yaoa, Y.-D. Zhangb, J. Lib, D.-T. Chenc, H.-T. Yina, C.-Q. Yub, P. Yuanb, Study of the nonlinear optical properties and behavior in phenoxy-phthalocyanines liquid at nanosecond laser pulses, Opt. Mater. 37 (2014) 80–86.
[14] N.S.K. Gowthaman, M. Amal Raj, S. Abraham John, Nitrogen-doped graphene as a robust scaffold for the homogeneous deposition of copper nanostructures: a nonenzymatic disposable glucose sensor, ACS Sustainable Chem. Eng. 5 (2017) 1648–1658.
[15] V. Balakumar, P. Prakash, P. Sathish Kumar, A new in-situ synthesized ternary CuNPs-PANI-GO nano composite for selective detection of carcinogenic hydrazine, Sens. Actuat. B 245 (2017) 156–165.
[16] A. Baishnisha, P. Selvakumar, Shen-Ming Chen, V. Vijayalakshmi, Te-Wei Chiu, Tse-Wei Chen, R. Sayee Kannan, A non-enzymatic amperometric hydrogen peroxide sensor based on iron nanoparticles decorated reduced graphene oxide nanocomposite, J. Colloid Interface Sci 487 (2017) 370–377.
[17] S. Chowdhury, R. Balasubramanian, Three-dimensional graphene-based porous adsorbents for postcombustion CO_2 capture, Ind. Eng. Chem. Res. 55 (2016) 7906–7916.
[18] V. Balakumar, P. Prakash, A facile in situ synthesis of highly active and reusable ternary Ag-PPy-GO nanocomposite for catalytic oxidation of hydroquinone in aqueous solution, J. Catal. 344 (2016) 795–805.
[19] M. Shtein, R. Nadiv, M. Buzaglo, O. Regev, Graphene-based hybrid composites for efficient thermal management of electronic devices, ACS Appl. Mater. Interfaces 7 (2015) 23725–23730.
[20] W.K. Chee, H.N. Lim, Z. Zainal, N.M. Huang, I. Harrison, Y. Andou, Flexible graphene-based supercapacitors: a review, J. Phys. Chem. C 120 (2016) 4153–4172.
[21] M.A. Ali, C. Singh, K. Mondal, S. Srivastava, A. Sharma, B.D. Malhotra, Mesoporous few-layer graphene platform for affinity biosensing application, ACS Appl. Mater. Interfaces 8 (2016) 7646–7656.
[22] M. Tanhaei, A.R. Mahjoub, V. Safarifard, Sonochemical synthesis of amide-functionalized metal-organic framework/graphene oxide nanocomposite for the adsorption of methylene blue from aqueous solution, Ultrason. Sonochem. 41 (2018) 189–195.
[23] C. Medina, Electronic tongue formed by sensors and biosensors containing phthalocyanines as electron mediators. Application to the analysis of red grapes, J. Porphyr. Phthalocya. 18 (2014) 76–86.
[24] D.D. Erbahar, M. Harbeck, I. Gürol, G. Gümüs, E. Musluoglu, Z.Z. Öztürk, V. Ahsen, Zinc phthalocyanines with fluorinated substituents for direct sensing of carbamate and organophosphate pesticides in water, J. Porphyr. Phthalocya. 17 (2013) 989–995.
[25] R. Jaisutti, T. Osotchan, An investigation of molecular interactions between zinc phthalocyanine thin film and various oxidizing gases for sensor applications, Adv. Mater. Res 403–408 (2012) 48–51.
[26] D. Rajkumar, K. Chelladurai, S.-M. Chen, P. Selvakumar, B.-S. Lou, M.A. Ali, F.M.A. Al-Hemaid, A sensitive and selective enzyme-free amperometric glucose biosensor using a composite from multi-walled carbon nanotubes and cobalt phthalocyanine, RSC Adv. 5 (2015) 26762–26768.
[27] D. Liu, Y.-T. Long, Superior catalytic activity of electrochemically reduced graphene oxide supported iron phthalocyanines toward oxygen reduction reaction, ACS Appl. Mater. Interfaces 7 (2015) 24063–24068.
[28] N.G. Mphuthi, A.S. Adekunle, E.E. Ebenso, Electrocatalytic oxidation of epinephrine and norepinephrine at metal oxide doped phthalocyanine/MWCNT composite sensor, Sci. Rep. 6 (2016) 26938.
[29] Y. Wang, N. Hu, Z. Zhou, D. Xu, Z. Wang, Z. Yang, H. Wei, E.S. Kong, Y.F. Zhang, Single-walled carbon nanotube/cobalt phthalocyanine derivative hybrid material: preparation, characterization and its gas sensing properties, J. Mater. Chem. 21 (2011) 3779–3787.
[30] B. Wang, X.Q. Zhou, Y.Q. Wu, Z.M. Chen, C.Y. He, Lead phthalocyanine modified carbon nanotubes with enhanced NH_3 sensing performance, Sens. Actuat. B 171–172 (2012) 398–404.
[31] J. Malig, N. Jux, D. Kiessling, J.-J. Cid, P. Vazquez, T. Torres, D.M. Guldi, Towards tunable graphene/phthalocyanine–PPV hybrid systems, Angew. Chem. Int. Ed. 50 (2011) 3561–3565.
[32] X. Zhou, X. Wang, B. Wang, Z. Chen, C. He, Y. Wu, Preparation, characterization and NH_3-sensing properties of reduced graphene oxide/copper phthalocyanine hybrid, Sens. Actuat. B 193 (2014) 340–348.
[33] H. Yu, B. Zhang, C. Bulin, R. Li, R. Xing, High-efficient synthesis of graphene oxide based on improved hummers method, Sci. Rep. 6 (2016) 36143.
[34] Z. Li, C. He, Z. Wang, Y. Gao, Y. Dong, C. Zhao, Z. Chen, Y. Wu, W. Song, Ethylenediamine-modified graphene oxide covalently functionalized with a tetracarboxylic Zn(II) phthalocyanine hybrid for enhanced nonlinear optical properties, RSC Photochem. Photobio. Sci. 15 (2016) 910–919.
[35] Z. Wang, C. He, W. Song, Y. Gao, Z. Chen, Y. Dong, C. Zhao, Z. Li, Y. Wu, The effect of peripheral substituents attached to phthalocyanines on the third order nonlinear optical properties of graphene oxide–zinc(II)phthalocyanine hybrids, RSC Adv. 5 (2015) 94144–94154.
[36] D. Chauhan, P. Kumar, G. Singh, D. Tripathi, S.L. Jain, Photo-assisted oxidation of thiols to disulfides using cobalt “Nanorust” under visible light, RSC Adv. 2 (2014) 50331–50337.
[37] S. Selvarajan, A. Suganthi, M. Rajarajan, K. Arunprasath, Highly efficient $BiVO_4$/WO_3 nanocomposite towards superior photocatalytic performance, Powder Technol. 307 (2017) 203–212.
[38] X. Feng, X. Ding, L. Chen, Y. Wu, L. Liu, M. Addicoat, S. Irle, Y. Dong, D. Jiang, Two-dimensional artificial light-harvesting antennae with predesigned high-order structure and robust photosensitising activity, Sci. Rep. 6 (2016) 32944.
[39] S. Srivastava, M.A. Ali, P.R. Solanki, P.M. Chavhan, M.K. Pandey, A. Mulchandani, A. Srivastava, B.D. Malhotra, Mediator-free microfluidics biosensor based on titania–zirconia nanocomposite for urea detection, RSC Adv. 3 (2013) 228–235.
[40] M. Tyagi, M. Tomar, V. Gupta, NiO nanoparticle-based urea biosensor, Biosens. Bioelectron. 41 (2013) 110–115.
[41] A.L. Ndiaye, S. Delile, J. Brunet, C. Varenne, A. Pauly, Electrochemical sensors based on screen-printed electrodes: the use of phthalocyanine derivatives for application in VFA detection, Biosensors 6 (2016) 46.
[42] I.S. Hosu, Q. Wang, A. Vasilescu, S.F. Peteu, V. Raditoiu, S. Railian, V. Zaitsev, K. Turcheniuk, Q. Wang, M. Li, R. Boukherrouba, S. Szunerits, Cobalt phthalocyanine tetracarboxylic acid modified reduced graphene oxide: a sensitive matrix for the electrocatalytic detection of peroxynitrite and hydrogen peroxide, RSC Adv. 5 (2015) 1474–1484.
[43] N. Rajesh, S.K. Puri, M.J. Mishra, A.K. Laskar, Srivastava, microstructural and potential dependence studies of urease-immobilized gold nanoparticles-polypyrrole composite film for urea detection, Appl. Biochem. Biotechnol. 172 (2014) 1055–1069.
[44] W. Hao, G. Das, H.H. Yoon, Fabrication of an amperometric urea biosensor using urease and metal catalysts immobilized by a polyion complex, J. Electroanal. Chem. 747 (2015) 143–148.
[45] R. Rahmanian, S.A. Mozaffari, Electrochemical fabrication of ZnO-polyvinyl alcohol nanostructured hybrid film for application to urea biosensor, Sens. Actuat. 207 (2015) 772–781.
[46] M. Dervisevic, E. Dervisevic, M. Şenel, Design of amperometric urea biosensor based on self-assembled monolayer of cystamine/PAMAM-grafted MWCNT/Urease, Sens. Actuat. 254 (2018) 93–110.
[47] S.G. Ansari, Rizwan Wahab, Z.A. Ansari, Young-Soon Kim, Gilson Khang, A. Al-Hajry, Hyung-Shik Shin, Effect of nanostructure on the urea sensing properties of sol–gel synthesized ZnO, Sens. Actuat. B 137 (2009) 566–573.
[48] M. Tak, V. Gupt, M. Tomar, Zinc oxide–multiwalled carbon nanotubes hybrid nanocomposite based urea biosensor, J. Mater. Chem. B 1 (2013) 6392–6401.
[49] Esteban Piccinini, Christina Bliem, Ciril Reiner-Rozman, Fernando Battaglini, Omar Azzaroni, Wolfgang Knoll, Biosens. Bioelectron. 92 (2017) 661–667.
[50] G. Das, H.H. Yoon, Amperometric urea biosensors based on sulfonated graphene/polyaniline nanocomposite, Int. J. Nanomed. 10 (2015) 55–66.
[51] K. Saeedfar, L.Y. Heng, T.L. Ling, M. Rezayi, Potentiometric urea biosensor based on an immobilized fullerene-urease bio-conjugate, Sensors 13 (2013) 16851–16866.
[52] P. Dasa Sarkar, Enzymatic electrochemical biosensor for urea with a polyaniline grafted conducting hydrogel composite modified electrode, RSC Adv. 6 (2016) 92520–92533.
[53] F. Branzoi, V. Branzoi, A. Musina, Amperometric urea biosensor based on platinum electrode modified with a nanocomposite film, Surf. Interf. Anal. 44 (2012) 895–898.
[54] R.K. Srivastava, S. Srivastava, T.N. Narayanan, B.D. Mahlotra, R. Vajtai, P.M. Ajayan, A. Srivastava, Functionalized multilayered graphene platform for urea sensor, ACS Nano 6 (2012) 168–175.
[55] R. Rahmanian, S.A. Mozaffari, M. Abedi, Disposable urea biosensor based on nanoporous ZnO film fabricated from omissible polymeric substrate, Mater. Sci. Eng. C 57 (2015) 387–396.
[56] N. Nguyen, G. Das, H.H. Yoon, Nickel/cobalt oxide-decorated 3D graphene nanocomposite electrode for enhanced electrochemical detection of urea, Biosens. Bioelectron. 77 (2016) 372–377.
[57] S. Abraham, V. Ciobota, S. Srivastava, S.K. Srivastava, R.K. Singh, J. Dellith, B.D. Malhotra, M. Schmitt, J. Popp, A. Srivastava, Mesoporous silica particle embedded functional graphene oxide as an efficient platform for urea biosensing, Anal. Methods 6 (2014) 6711–6720.